Journal Article

Protein/polysaccharide intramolecular electrostatic complex as superior food-grade foaming agent

Xu, Y., Yang, N., Yang, J., Hu, J., Zhang, K., Nishinari, K., Phillips, G.O., Fang, Y

Journal Pre-proof

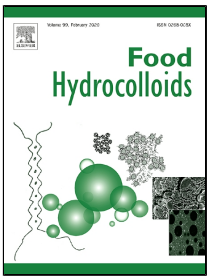

Protein/Polysaccharide Intramolecular Electrostatic Complex as Superior Food-Grade Foaming Agent

Yao Xu, Nan Yang, Jixin Yang, Jing Hu, Ke Zhang, Katsuyoshi Nishinari, Glyn O. Phillips, Yapeng Fang

PII:	S0268-005X(19)31840-5
DOI:	https://doi.org/10.1016/j.foodhyd.2019.105474
Reference:	FOOHYD 105474
To appear in:	*Food Hydrocolloids*
Received Date:	11 August 2019
Accepted Date:	29 October 2019

Please cite this article as: Yao Xu, Nan Yang, Jixin Yang, Jing Hu, Ke Zhang, Katsuyoshi Nishinari, Glyn O. Phillips, Yapeng Fang, Protein/Polysaccharide Intramolecular Electrostatic Complex as Superior Food-Grade Foaming Agent, *Food Hydrocolloids* (2019), https://doi.org/10.1016/j.foodhyd.2019.105474

Graphical abstract

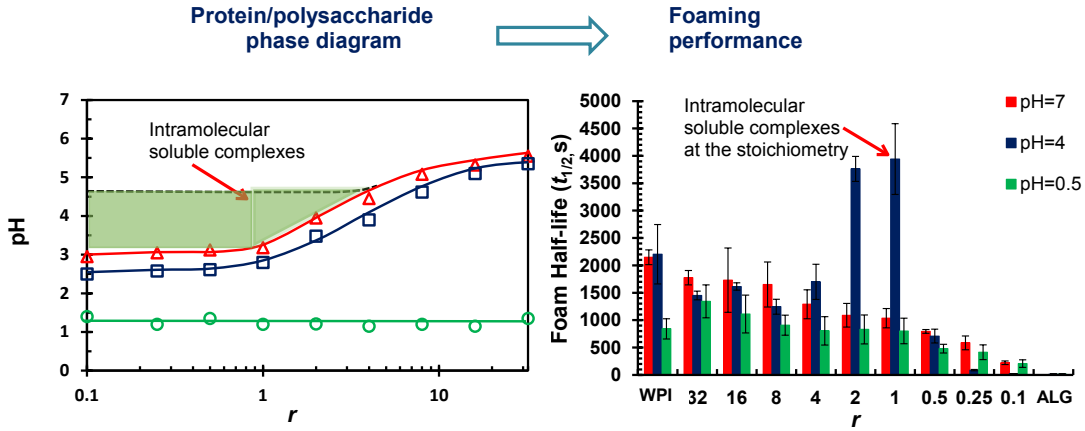

Protein/Polysaccharide Intramolecular Electrostatic Complex as Superior Food-Grade Foaming Agent

Yao Xu [a, ‡], Nan Yang [a, ‡], Jixin Yang [b], Jing Hu [a], Ke Zhang [a], Katsuyoshi Nishinari [a], Glyn O. Phillips [a], Yapeng Fang [, c]*

[a] Glyn O. Phillips Hydrocolloid Research Centre, School of Food and Biological Engineering, Hubei University of Technology, Wuhan 430068, China.

[b] Faculty of Arts, Science and Technology, Glyndwr University, Mold Road, Wrexham, LL11 2AW, UK.

[c] Department of Food Science and Technology, School of Agriculture and Biology, Shanghai Jiao Tong University, Shanghai 200240, China.

[‡] Equal contributions.

[*]Corresponding author: Tel/Fax, +86-(0)-21-34208547; Email, ypfang@sjtu.edu.cn.

Abstract: High-performance foaming agents are widely required in the food industry. In this study, the relationship between electrostatic interaction of whey protein isolate (WPI)/alginate (ALG) and the resultant foaming properties were investigated systematically. The phase diagram of WPI/ALG was established in terms of protein/polysaccharide mixing ratio (r) and pH. The results show that the foaming capacity of WPI/ALG complexes is almost the same across different regions of the phase diagram, while the foam stability varies significantly. At pHs 7.0 and 0.5 where no electrostatic complexation occurs, the foam stability is found to decrease monotonically with decreasing r. At pH 4.0 and particular mixing ratios, i.e., r = 1 and 2, intramolecular soluble complexes are formed and the particular WPI/ALG complexes yield the best foam stability, as compared to other electrostatic complexes or individual components. The half-life ($t_{1/2}$) of the foams stabilized by the intramolecular electrostatic complexes is as long as 4000 s at a very low WPI/ALG concentration of 0.1% w/w. The foaming properties are in line with the foam viscosity, interfacial adsorption behavior and microstructures of the complexes observed at the air-water interface. This demonstrates that the protein/polysaccharide intramolecular electrostatic complex, more specifically at the stoichiometry, could potentially act as a superior foaming agent in the food industry.

Keywords: Intramolecular Electrostatic Complex, Phase Diagram, Whey Protein Isolate, Alginate, Foam Capacity, Foam Stability

1. Introduction

Foam is universally present in our daily life and it plays a crucial role in various applications such as foods, detergents, pharmaceuticals, cosmetics, ultra-light materials and fire-fighting agents etc (Zang, et al., 2018). Foam is particularly common and important in the food industry, and is one of the most vital ingredients in some specific food products, owing to its ability to provide special structures, appearance and tastes (Dickinson, 2010; van Kempen, Schols, Van, & Sagis, 2013). These include bread, sponge cakes, ice creams, mousses and chocolates(Langevin, et al., 2005). Foam structures are usually stabilized by surfactants, proteins, fats and even alcohols, and the stability of foams is characterized by their half-life. Long-life foams which normally last 50 minutes or longer (Piazza, Gigli, & Bulbarello, 2008) are particularly useful for aerated products in the food industry due to their ability of maintaining desired appearance of foods (Raikos, Campbell, & Euston, 2007). Therefore, all-natural, green-label and healthy foaming agents with superior performance can make great contribution to the food industry.

Proteins represent the major category of natural foaming agents in the food industries (Hill & Eastoe, 2017). Proteins typically used for foaming purposes include β-lactoglobulin (Dombrowski, Gschwendtner, & Kulozik, 2017; Peng, Yang, Li, Tang, & Li, 2017), whey protein (Oboroceanu, Wang, Magner, & Auty, 2014), egg white protein (Mitie S. Sadahira, Rodrigues, Akhtar, Murray, & Netto, 2016) and wheat gluten protein (Wouters, et al., 2017), etc. However, some proteins have certain limitations either in foam capacity or foam stability, which cannot meet the requirements of the increasingly fastidious food industry. For instance, native whey proteins showed inferior foam capacity and stability at different pHs and concentrations when compared with denatured whey proteins (Oboroceanu, et al., 2014). For this reason, continuous effort has been made to seek for

methodologies that improve the foaming properties of food proteins. Experimental factors, such as temperature (Z. Wan, Yang, & LM, 2016), pH (Peng, et al., 2017), concentration (Oboroceanu, et al., 2014), and ionic strength (Akkermans, Goot, Venema, Linden, & Boom, 2008), were reported to influence the foaming properties. For example, Oboroceanu *et al*. (2014) found that whey protein isolate fibrils formed at lower pH and higher temperature exhibited greater foaming capacity and stability than the native protein. Peng *et al*. (2017) found that β-lactoglobulin amyloid fibrils had better foam capacity at pH = 7-8 than at other pHs. However, when the pH was close to its isoelectric point, the foam generated by the β-lactoglobulin amyloid fibrils gave the highest stability due to the lower electrostatic repulsion and hence a tightly packaged adsorption layer at the air-water interface.

The foaming properties of proteins can also be improved by combination with polysaccharides (Jarpa-Parra, Tian, Temelli, Zeng, & Chen, 2016) since protein-polysaccharide complexation at the air/water interface efficiently enhances the foam stability (Miquelim, Lannes, & Mezzenga, 2010). Proteins and polysaccharides can form complexes of different states at various pHs and mixing ratios. These include individual soluble polymers, intramolecular soluble complexes, intermolecular soluble complexes and intermolecular insoluble complexes (Li, Fang, Al-Assaf, Phillips, Yao, et al., 2012), which could influence the foaming properties of proteins to different degrees. In recent years, the influence of polysaccharides on protein foaming properties has been investigated extensively (Narchi, Vial, & Djelveh, 2009; Juan Miguel Rodríguez Patino & Pilosof, 2011; M. S. Sadahira, et al., 2015; van den Berg, Jara, & Pilosof, 2015). Most of the studies were focused on the effects of protein-polysaccharide interactions at certain pHs (Ruíz Henestrosa, Carrera-Sánchez, & Patino, 2008) or the type and concentration of polysaccharides (Mitie S. Sadahira, et al., 2016). For example, Jarpa-Parra *et al*. (Jarpa-Parra, et al., 2016) demonstrated that lentil legumin-like proteins exhibited a

higher foam stability in the presence of guar gum, xanthan gum and pectin at pH 5.0 than pH 3.0 and 7.0. Moreover, the polysaccharides were different in terms of their effects.

Our previous study has investigated the emulsifying performance of different types of protein-polysaccharide complexes and demonstrated that the intramolecular soluble complexes could greatly improve the stability of emulsions due to the cooperative adsorption of protein and polysaccharide at the oil-water interface and the resulting thick interfacial adsorption layer around the droplet surface (Li, Fang, Al-Assaf, Phillips, & Jiang, 2012). The formation and stabilization of foams are also expected to closely relate with the interfacial adsorption of foaming agents, although not exactly the same to the case of emulsion stabilization (Foegeding, Luck, & Davis, 2006). In view of this, we herein investigate systematically the foams stabilized by different types of protein-polysaccharide electrostatic complexes, with particular emphasis on the intramolecular soluble complexes. Many studies demonstrate that whey protein isolate (WPI) can be used as an effective foaming agent to improve the quality of foamed foods such as texture and volume (Davis & Foegeding, 2004; Kuropatwa, Tolkach, & Kulozik, 2009; Vaclavik & Christian, 2008). Alginate (ALG) is a linear anionic polysaccharide (Draget, Phillips, & Williams, 2009), and has been widely used in the pharmaceutical and food industries (Stender, et al., 2018). In the work, WPI and ALG are selected to produce different types of electrostatic complexes according to a phase diagram, and the resultant foaming properties are comparatively studied by measuring foaming capacity and stability.

2. Material and methods

2.1 Materials

Whey protein isolate (WPI) BiPRO® (98% w/w) mainly consisting of 65% β-lactoglobulin, 25% α-lactoglobulin and 8% bovine serum albumin was kindly provided by Davisco Foods International Inc., (Le Sueur, MN, USA). The molecular weight and mean square radius of gyration (R_g) of WPI are 2.0 × 10^4 Da and 11 nm, respectively. Sodium alginate (ALG) with a weight-average molecular mass of Mw = 2.3 × 10^5 Da and R_g = 78.8 nm (100% w/w) was obtained from FMC BioPolymer (Norway). D-glucono-δ-lactone (GDL) was purchased from Aladdin Chemistry (China). All other chemicals were of analytical grade. Ultrapure water of Milli-Q system (18.3 MΩ.cm) was used for sample preparation.

2.2. Preparation of protein/polysaccharide mixtures

Sodium alginate was purified by precipitation using absolute ethyl alcohol, followed by re-dissolution, dialyzing and freeze-drying. Stock solutions of WPI (0.1% w/w) and ALG (0.1% w/w) were prepared by dissolving appropriate amount of WPI and ALG, respectively, in Millipore water. The stock solutions were mixed at different proportions under magnetic stirring to yield different mixing ratios of WPI/ALG by weight. WPI, ALG and WPI/ALG mixtures at pHs = 0.5, 4.0 and 7.0 were used for further study of foaming properties. The pH was adjusted using HCl (1 M) and NaOH (1 M).

2.3. Zeta potential measurements

ζ-potential within the pH range of 2.0-8.0 were measured using a Zetasizer Nano-ZS apparatus (Malvern Instruments, UK) equipped with an MPT-2 pH autotitrator. The apparatus was fixed with a 4 mW He/Ne laser emitting at 633 nm (Yao, et al., 2016). ζ potential was determined by measuring the actual electrophoretic mobility U_E of charged particles via laser Doppler velocimetry at an angle

of 17° according to the equation (Li, Fang, Al-Assaf, Phillips, Yao, et al., 2012):

$$= 3\eta U_E/2\varepsilon f(Ka) \quad (1)$$

where ε is the dielectric constant and η is the viscosity of the medium. $f(Ka)$ is the Henry function which is close to 1.5 under the Smoluchowski approximation.

2.4. Construction of phase diagram

The phase diagram of WPI/ALG mixtures was constructed at various mixing ratios by measuring light scattering and turbidity during *in situ* acidification using GDL, as described previously (Li, Fang, Al-Assaf, Phillips, Yao, et al., 2012; Mekhloufi, Sanchez, & Renard, 2005; F Weinbreck, De, Schrooyen, & de Kruif, 2003). Briefly, 10 grams of 0.1% WPI/ALG solution was adjusted to pH 9.0, and then mixed vigorously with different amounts of GDL ranging from 0.25 to 2.0 % w/w to initialize *in situ* acidification (Li, Fang, Al-Assaf, Phillips, Yao, et al., 2012). The change of pH as a function of time was recorded using an Orion 4 Star multifunctional pH meter (Thermo Scientific Corporation) at 25 °C. The pH-time curves were related to the subsequent time-dependent light scattering intensity and turbidity measurements to obtain the information on structural transitions as a function of pH (Li, Fang, Al-Assaf, Phillips, Yao, et al., 2012).

Light scattering was measured on a Zetasizer apparatus (Malvern Instruments, UK). The average scattered light intensity at 173° (I_{173}, counts s^{-1}) was recorded every 30 s for 5 hours during *in situ* acidification at 25 °C. Turbidity measurement was carried out on a UV/visible spectrophotometer (TU-1900, PERSEE, China) at a wavelength of 500 nm. The turbidity (τ, cm^{-1}) was recorded every 30 s for 5 hours and was calculated according to the equation (Yao, et al., 2016):

$$\tau = (1/L) \ln (I_0/I_t) \quad (3)$$

where L is the optical path length (cm), I_0 and I_t are the incident and transmitted light intensity, respectively. Since the GDL-induced acidification could not bring pH below 2.0, 10 M HCl was used instead to decrease pH from 6.0 to 1.0 in parallel experiments.

2.5. Analysis of foaming properties

Dynamic foam properties (foam capacity and foam stability) of WPI/ALG mixtures were analyzed using a dynamic foam analyzer DFA100 (KRÜSS GmbH, Germany). Changes in total height and foam structure over time were measured simultaneously. For each measurement, a fixed volume of WPI, ALG or WPI/ALG (50 mL) was foamed to a maximum height of 180 mm by sparging air (0.3 L/min) in a tempered glass column with a prism comprised over the whole length of the column (height = 250 mm; inner diameter = 40 mm) through a porous filter plate (16-40 μm). Two-dimensional images of foams for each sample at a column height of 80 mm after foaming were taken by a CCD camera that was attached to the side of prism of the column. The detailed principle for monitoring the foam structure can be found from Oetjen et al (Oetjen, Bilke-Krause, Madani, & Willers, 2014). The results of high contrast images were analyzed by the Foam Analysis Software. In general, dynamic foam analyzer consisted of a foam generation device and a computer which served as the data acquisition and monitoring unit. Foam capacity was defined as follows:

$$\text{Foam Capacity} = V(\text{Foam}, t_{max}) / V(\text{Gas}) \quad (4)$$

where V (Foam, t_{max}) is the maximum foam volume reached at time t_{max}, and V (Gas) is the volume of gas consumed until t_{max}. The foam stability (FS) was characterized by the half-life of foam ($t_{1/2}$), i.e., the time over which the foam height is reduced to one-half of its initial value.

2.6. Rheological measurements

The viscosity (η) of the WPI/ALG solutions with different protein/polysaccharide ratio r (at a fixed total biopolymer concentration of 0.1% w/w) was measured at 25 °C using a Haake RheoStress 6000 rheometer (Thermo Fisher Scientific, USA) with a parallel-plate geometry. The plate diameter and the gap between top and bottom plates are 35 mm and 1.0 mm, respectively. The shear rate range investigated was from 0.01 to 100 s^{-1}.

2.7. Surface tension and dilatational rheology

The surface tension and dilatational modulus (E) of WPI/ALG at the air-water surface were measured through oscillation mode by a drop profile tensiometer (Teclis Tracker, France). The experiments were carried out at 25 ± 0.1°C controlled by a water bath circulation. A thoroughly cleaned syringe with a U-shaped needle was submerged into a quartz sample cell containing WPI, ALG or WPI/ALG solution (0.1% w/w). The sample cell was situated between a light source and a high-speed charge couple device (CCD) camera. A bubble with a volume of 5 μL (A) was produced in the WPI, ALG or WPI/ALG solution at the tip of the needle. The surface area of the bubble was sinusoidally fluctuated with time (t) at an oscillation frequency of 0.05 Hz and a relative amplitude of 10% ($\Delta A/A$) for a duration of 3.5 h. The bubble profile was recorded by the CCD camera and analyzed according to the equation derived from Laplace equation: (Castellani, Al-Assaf, Axelos, Phillips, & Anton, 2010; Castellani, Gaillard, et al., 2010; Castellani, Guibert, et al., 2010)

$$\frac{1}{x}\frac{d}{dx}(\mathrm{x}\sin\theta) = \frac{2}{b} - cz \qquad (5)$$

where x and z are the Cartesian coordinates at any point on the drop profile, b is the curvature radius at the drop apex, θ is the angle of the tangent to the drop profile and c is the capillarity constant $g\Delta\rho/\gamma$ ($\Delta\rho$ is the density difference between air and solution, γ is the interfacial tension and g is the

acceleration of gravity, respectively). The surface dilatational modulus E was calculated as follows:

$$E = A(\Delta\gamma) / \Delta A \quad (6)$$

where A and ΔA are the initial surface area of the bubble and its oscillation amplitude.

2.8. Atomic force microscopy (AFM)

The microstructures of WPI, ALG or WPI/ALG at the air-water interface were visualized using a MuitiMode 8 scanning probe microscopy (Bruker, USA) in Peak Force Tapping Mode in air. AFM images were recorded with a silicone cantilever (driving frequency 70 kHz; spring constant 0.4 N/m). AFM samples were prepared according to a modified Langmuir-Schaefer method to transfer interfacial films on to freshly cleaved micas (Jordens, Isa, Usov, & Mezzenga, 2013). WPI and ALG stock solutions of 0.01 mg/mL were prepared by dispersing the respective powders in Milli-Q water under magnetic stirring overnight and then mixed at different weight ratios at pH 4.0 and pH 7.0. 10 mL of the mixed solutions was transferred to a flat glass dish (depth = 15 mm and inner diameter = 50 mm) and allowed to stand for an hour. A freshly cleaved mica nipped using a tweezer was brought down to contact with the air-water interface and then withdrawn rapidly again. The mica was dried for 12 hours under ambient condition prior to AFM observation.

2.9. Statistical analysis

Independent experiments for each sample were repeated in triplicate. The average values and the standard deviation (SD) are reported using descriptive statistical analysis, which was performed through Excel 2013.

3. Results and discussion

3.1. Zeta potential of WPI/ALG mixtures

ζ-potential of WPI/ALG with varying protein/polysaccharide ratios (*r*) and as a function of pH is shown in Fig. 1a. The WPI solution shows an isoelectric point (IEP) of 4.61, which agrees with the reported value in the literature (F Weinbreck, et al., 2003). The ALG solution attains a saturated ζ value of -50 mV at pH > 6.0, and approaches zero when the pH is reduced to 2.0 due to the protonation of carboxylic groups around their pKa (Li, Fang, Al-Assaf, Phillips, Yao, et al., 2012). For WPI/ALG mixtures, decreasing *r* results in a shift of ζ curves to lower pHs and therefore a lower IEP for WPI/ALG mixtures than pure WPI. Fig. 1b plots the IEP values of the WPI/ALG mixtures against *r*. Obviously, IEP shows a clear transition around $r = 1.0$, and is nearly constant at $r < 1.0$. This suggests that the maximum stoichiometry of WPI/ALG is approximately 1.0. This weight ratio indicates that one gram of ALG to a maximum can interact with WPI of the same weight (Li, Fang, Al-Assaf, Phillips, Yao, et al., 2012). In other words, when $r > 1.0$, the possible binding sites of ALG are fully occupied by WPI molecules (Vinayahan, Williams, & Phillips, 2010). When $r < 1.0$, the ALG is in excess, and the free carboxylic groups unoccupied by WPI dominate the IEP of the mixtures through a protonation mechanism.

(Fig. 1. here)

3.2. Phase diagram of WPI/ALG

In order to construct the phase diagram of WPI/ALG mixtures, light scattering and turbidimetry were employed to monitor the structure transitions during GDL-induced acidification (Li, Fang, Al-Assaf, Phillips, Yao, et al., 2012). Fig. 2a takes $r = 1$ as an example to illustrate the evolution of turbidity at 500 nm (τ), scattered light intensity at 173° (I_{173}) as a function of pH. Two characteristic

pHs can be identified from the evolution profiles: pH_c as the onset increase of I_{173} and pH_φ as the onset increase of τ (Mekhloufi, et al., 2005; Ye & Flanagan, 2006). As can be seen in Fig. 2a, I_{173} and τ keep constant when $pH > pH_c$ and I_{173} starts to increase at $pH < pH_c$. When $pH_\varphi < pH < pH_c$, τ remains unchanged, but starts to ascend dramatically at pH_φ. pH_c has been regarded as an indication of the formation of soluble complexes and pH_φ is associated with the formation of insoluble complexes which eventually leads to phase separation (Mekhloufi, et al., 2005; F Weinbreck, et al., 2003; Fanny Weinbreck, Nieuwenhuijse, Robijn, & de Kruif, 2004; Ye, et al., 2006). This is because I_{173} is more sensitive to the size change at the molecular level while τ probes the size change at the microscopic level (Li, Fang, Al-Assaf, Phillips, Yao, et al., 2012; Mekhloufi, et al., 2005).

(Fig. 2. here)

To analyze the structure transition at lower pHs where the GDL acidification cannot reach, HCl addition was used to acidify pH until below pH 1.0 meanwhile measuring the turbidity change (Li, Fang, Al-Assaf, Phillips, Yao, et al., 2012). As can be seen in Fig. 2a, further decreasing pH by HCl leads to a reduction in turbidity. At $pH < pH_d$, the turbidity starts to level off, but does not disappear completely. This is different from the system of bovine serum albumin/sugar beet pectin in which the turbidity approached almost zero at $pH < pH_d$ (Li, Fang, Al-Assaf, Phillips, Yao, et al., 2012). The reason could be that such low pHs cause the protonation of carboxylic groups, and induce the aggregation and microgel formation of ALG, thus giving rise to considerable turbidity. Nevertheless, the transition at pH_d is still associated with the dissociation of WPI/ALG complexes and the subsequent formation of ALG microgels due to the protonation of carboxylic groups (Li, Fang, Al-Assaf, Phillips, Yao, et al., 2012; Vinayahan, et al., 2010; Ye, et al., 2006).

Based on the pH_c, pH_φ and pH_d values identified at different mixing ratios, the phase diagram of WPI/ALG mixtures was constructed in a pH-composition coordinate as shown in Fig. 2b. Both pH_c

and pH_{φ} have a sigmoidal dependence on *r*, while the value of pH_d does not change much with *r*. At lower mixing ratios *r*, pH_c is significantly smaller than the IEP of WPI (indicated by the dashed line). Our previous study proved that between IEP and pH_c electrostatic complexation already occurs between WPI and ALG, leading to the formation of intramolecular soluble complexes (Li, Fang, Al-Assaf, Phillips, Yao, et al., 2012). The IEP, pH_c, pH_{φ} and pH_d divide the phase diagram into five regions, and according to the previous assignments they correspond to: (I) a stable region of mixed individual soluble polymers, (II) a stable region of intramolecular soluble complexes, (III) a metastable region of intermolecular soluble complexes, (IV) an unstable region of intermolecular insoluble complexes and (V) a second stable region of mixed individual soluble polymers, respectively (Li, Fang, Al-Assaf, Phillips, Yao, et al., 2012; Mekhloufi, et al., 2005; Seyrek, Dubin, Tribet, & Gamble, 2003). Since the intramolecular soluble complexes represent a stable state of the electrostatic complexation as demonstrated previously (Yao, et al., 2016), special emphasis will be put on their foaming properties in the following discussion.

3.3. Foaming properties

The foaming properties of WPI/ALG mixtures were investigated in terms of the phase diagram shown in Fig. 2b. WPI/ALG mixtures at pH 7.0, 4.0 and 0.5 and with varying mixing ratio from 0.1 to 32 were selected to evaluate the foam capacity and stability. The experimental conditions ensure a complete coverage of the different phase regions in the phase diagram. The foam capacity was assessed by the ratio of the maximum foam volume to the volume of gas consumed for foaming therein. Fig. 3 compares the foaming capacity of WPI/ALG mixtures of different mixing ratios at pHs 7.0, 4.0 and 0.5. At a fixed total biopolymer concentration of 0.1% w/w and higher mixing ratios, WPI/ALG mixtures exhibit comparable foam capacity with the pure WPI and among the three

different pHs. At pH 7.0 and 0.5 where no electrostatic complexation occurs, the foam capacity of WPI/ALG mixtures starts to decline significantly at $r < 0.1$ and 0.25, respectively. This is because the foam capacity is mainly determined by the amphiphilic protein component and it would decrease extensively when the amount of protein is reduced to a certain level at lower mixing ratio. At pH 4.0 where electrostatic complexation takes place, the foam capacity shows a marked decrease starting at $r < 1$. This critical r value coincides with the maximum stoichiometry of WPI/ALG as revealed in Fig. 1b, and is considerably larger than those observed for pH 7.0 and 0.5. A possible interpretation is that the electrostatic complexation between WPI and ALG reduces the amount of free protein that is required for effective foaming. Only when the mixing ratio is larger than the stoichiometry, that is, $r > 1$, does the presence of excessive free protein confer a good foam capacity. Overall, the results indicate that the addition of ALG, either in free state or complexed with WPI, does not lead to an improvement of the foam capacity of WPI. This is due to the hydrophilic nature of ALG, and is in line with the results obtained for other protein/polysaccharide systems (Jarpa-Parra, et al., 2016).

(Fig. 3. here)

Nevertheless, the foam stability was found to be significantly altered by the presence of ALG. Foam stability was evaluated by measuring the decay of the foam height over time and was quantified by the foam half-life, i.e., the time over which the foam height is reduced to one-half of its initial value. Fig. 4a exemplifies the decay of foam height as a function of time for WPI/ALG at pH 4.0 and various mixing ratios. Due to the drainage of the liquid, the foam height continues to decrease. It is clear that at particular mixing ratios, i.e., $r = 1$ and 2, the foams show the slowest decay with time. When $r < 1$, the foam decay is accelerated with decreasing mixing ratio. Fig. 4b compares the foam half-life for WPI/ALG at different pHs and mixing ratios. At pHs 7.0 and 0.5 where no electrostatic complexation occurs, the foam half-life decreases monotonically with

decreasing *r*. This is readily understood, as the decreasing amount of free protein results in insufficient coverage of the water-air interface by WPI and thus the destabilization of the foams. Additionally, the foam half-life at pH 0.5 seems to be slightly shorter than that at pH 7.0. This could be caused by the deamidation of amino acids and hydrolysis of peptide bonds of WPI at pH 0.5, which alter the covalent structure and amphiphilicity of WPI and have a detrimental effect on foam stability.

(Fig. 4. here)

At pH 4.0 where electrostatic complexation takes place between WPI and ALG, the foam half-life generally decreases with decreasing *r*, but goes through a substantial maximum around $r = 1$. The foam half-life at $r = 1$ and 2 is as long as 4000 s, which nearly doubles that of pure WPI even if the protein concentration is reduced to only the half. This suggests clearly an improvement of the foam stability by electrostatic complexation with ALG. Intriguingly, the maximum foam stability occurs at $r = 1$ and 2, which is close to the stoichiometry of WPI/ALG and falls within the stable region of intramolecular soluble complexes, as shown in the phase diagram (Fig. 2b). This manifests an extraordinary foam-stabilizing effect of the intramolecular soluble complex around its stoichiometry. For intramolecular complex with $r < 1$, because of the deviation from the stoichiometry, excessive ALG renders the complexes highly negatively charged, which impairs their adsorption and structural arrangement at the air-water interface due to strong electrostatic repulsion (Mitie S. Sadahira, et al., 2016). This results in a decreased foam stability at lower mixing ratio. On the other hand, for $r > 2$, the WPI/ALG mixtures enter into the metastable region of intermolecular soluble complexes or the unstable region of intermolecular insoluble complexes (Fig. 2b). The formation of unstable intermolecular complexes of WPI/ALG may cause the destabilization of the air-water interface since the intermolecular complexes form insoluble complexes and sediment, thus reducing the interfacial

properties and the viscosity of the complex system (as discussed below), and likely causing the coalescence of air bubbles. This explains the lower foam stability observed at higher mixing ratio.

(Fig. 5. here)

The time evolution of foam structure was monitored by a CCD camera during foam formation and decay (Fig. 5). At the very beginning, e.g., 30s, all the foams formed at pH 7.0, 4.0 and 0.5 contain nearly monodisperse and small spherical air bubbles. With the elapse of time, the bubbles grow in size due to destabilizations such as disproportionation and coalescence. As the liquid continues to drain, the bubbles become compressed and start to pack together in a polyhedral shape (Zhili Wan, Yang, & Sagis, 2016). Comparison between pH 7.0 and 0.5 shows that the foams formed at pH 0.5 have relatively smaller initial bubble size, which however seem to grow more rapidly. At 3000s, the foams formed at pH 0.5 dry out completely, while the foams at pH 7.0 can partially retain the polyhedral structure. This means that the foams formed at pH 7.0 are more resistant to foam drainage than those at pH 0.5, indicating a slightly higher foam stability. Great difference can be seen at pH 4.0 where WPI and ALG complex with each other via electrostatic interaction. At particular mixing ratios, i.e., r = 1 and 2, the bubbles have a smaller initial size, and grow relatively more slowly in comparison with the bubbles formed at other mixing ratios. Moreover, most of the bubbles can remain spherical even at 3000 s, with only a few in the polyhedral shape. This is in clear contrast with the foams formed at pH 7.0 and 0.5, and indicates a much stronger resistance to foam drainage (Zhili Wan, et al., 2016). The foam microstructures confirm that the intramolecular soluble complex around its stoichiometry possesses an excellent ability of stabilizing foams.

3.4. Viscosity

Foam drainage, one of the important factors influencing the foam stability, is deeply related to

viscosity of continuous phase of foam (Koehler, Sascha Hilgenfeldt, & Stone, 2000). Therefore, the viscosity profiles of WPI/ALG mixtures with varying *r* and at different pHs as a function of shear rate are measured and displayed in Fig. 6. The viscosity of all the samples presented a shear thinning behavior with the increase of shear rate from 0.01 to 100 s^{-1}, which has been observed in other protein/polysaccharide (Jarpa-Parra, et al., 2016) or protein alone systems (Peng, et al., 2017; Ptaszek, 2013). However, the initial viscosity and the decrease rate of viscosity varied among different WPI/ALG mixtures. In Fig. 6a, ALG at pH 7.0 showed the lowest viscosity at low shear rate (< 6 s^{-1}), while WPI exhibited the highest on the contrary. In general, the viscosity of WPI/ALG mixtures became lower with decreasing *r*. This viscosity change tendency implies that the viscosity is primarily influenced by WPI at pH 7.0, but the electrostatic repulsion between the biopolymer molecules becomes stronger at low *r* (Fig. 1a), leading to the decrease of viscosity (Peng, et al., 2017).

When pH is 4.0, as can be seen in Fig. 6b, ALG remains the smallest viscosity. Nevertheless, the intramolecular soluble polymers (*r* =1 and 2) and the intermolecular soluble polymers (*r* = 4) of WPI/ALG complexes at low shear rate (< 6 s^{-1}) showed higher viscosities than pure ALG. This might be because the formation of even-distributed primary coacervates (intramolecular soluble polymers) or small scale aggregates (intermolecular soluble polymers), respectively. As *r* further increases to *r* = 16 where intermolecular insoluble polymers are formed, viscosity decreases as expected since sedimentation may occur during the rheological tests. This phenomenon was also observed for other protein/polysaccharide complex system (Jarpa-Parra, et al., 2016). For WPI/ALG complexes with lower *r*, the high content of negatively charged ALG still show lower viscosity than the other WPI/ALG complexes.

At pH 0.5, however, an opposite viscosity trend of WPI/ALG mixtures as a function of *r* is

observed compared to that at pH 7.0 (Fig. 6c). That is, ALG had the largest viscosity and the viscosity of WPI/ALG mixtures becomes lower as *r* increases. This is probably because aggregation and microgel formation of ALG at very low pH (Su, et al., 2018) which dominate the viscosity change of the WPI/ALG systems.

(Fig. 6. here)

3.5. Interfacial properties

The foaming properties of proteins are relevant to their adsorption at the air-water interface (Wouters, et al., 2017). Therefore, the interfacial behavior of the WPI/ALG mixtures with varying mixing ratios at the air-water interface was investigated to deeply understand their foaming properties. Fig. 7 shows the time evolution of the surface tension and surface dilatational modulus (*E*) for WPI/ALG mixtures at the air-water interface at pH 4.0 and 7.0, respectively. The adsorption at pH 0.5 could not be measured properly. This is because ALG at pH 0.5 would be and form aggregated sediments in the sample tank during measurement, leading to inaccurate results. Similar problem was encountered during the measurements of WPI/ALG at higher mixing ratio and pH 4.0, i.e., $r > 4$, where WPI/ALG form insoluble complexes (region IV in Fig. 2b), preventing accurate characterization of the interfacial adsorption behavior.

(Fig. 7. here)

In Figs 7a and 7b, the surface tension of all the samples decreases with time, and tends to level off, implying the adsorption of WPI, WPI/ALG and even ALG to the air-water interface (Peng, et al., 2017). However, the decay rate of the surface tension is different for different samples, which indicates the difference in diffusion and adsorption rate of the samples. As displayed in Fig. 7a, at pH 7.0, the decay rate of the surface tension for pure ALG is the slowest and the equilibrium value

of the surface tension is the highest. It suggests that the polysaccharide ALG is not as surface-active as the samples containing the protein WPI. This is related to the poor hydrophobicity of ALG, which leads to slow interfacial adsorption kinetics and a low surface activity. On the contrary, WPI displays the fastest decay of surface tension and the lowest equilibrium value at the late stage of the adsorption, suggesting a higher surface activity of WPI (Bals & Kulozik, 2003; Davis, et al., 2004; Oboroceanu, et al., 2014). Additionally, the surface tension for WPI/ALG mixtures with different mixing ratios is in between the values for ALG and WPI, and decreases with decreasing *r*. The results indicate that the surface activity of WPI/ALG is dominated by WPI at pH 7.0, where no electrostatic complexation occurs.

At pH 4.0, as shown in Fig. 7b, ALG remains the slowest decrease rate and the highest equilibrium value of surface tension, implying a poor surface activity similar to that at pH 7.0. Interestingly, it was found that the WPI/ALG intramolecular soluble complex at $r = 1$, namely the stoichiometry, exhibits the lowest equilibrium surface tension and the fastest decay rate, in comparison with other mixtures and even pure WPI. This could be due to the fact that electrostatic complexation induces the partial denaturation of WPI, resulting in exposure of more hydrophobic regions of the protein and thus a higher surface activity (Cao, Li, Fang, Nishinari, & Phillips, 2016). Furthermore, the electrostatic complexation enhances the solubility of WPI due to increased electrostatic repulsion and promotes the cooperative adsorption of WPI and ALG on to the air-water interface, which give rise to a faster adsorption kinetics (Li, Fang, Al-Assaf, Phillips, & Jiang, 2012). The effects are the most pronounced at the stoichiometry $r = 1$. The deviation from the stoichiometry leads to either insufficient amount of proteins anchored to the interface (i.e., $r < 1$) or the metastable/unstable complexes that tends to aggregate/precipitate (i.e., $r > 1$). Neither of the

situations favors the adsorption of WPI/ALG onto to the air-water interface, leading to reduced surface activity.

Figs 7c and 7d show the corresponding surface dilatational modulus *E* of WPI/ALG mixtures at pHs 7.0 and 4.0, respectively. At pH 7.0, ALG exhibits the lowest *E* while WPI has the highest *E*. The *E* values for WPI/ALG mixtures with different mixing ratios are also in between those of pure WPI and ALG, and increase with increasing *r*. It implies that WPI at pH 7.0 forms the most viscoelastic surface film, and therefore should provide the highest foam stability. As *r* decreases, the viscoelasticity of the surface film formed by WPI/ALG mixtures declines. This explains the reduced foam stability as *r* decreases as observed in Fig. 4b and agrees with the results reported in literatures (Murray, 2011; J. M. Rodríguez Patino, Carrera, & Rodríguez Niño, 2008). At pH 4.0 (Fig. 7d), *E* is generally larger at higher *r*. However, exception is that the intramolecular soluble complexes at $r = 1$ or 2 display the highest *E* values which outstands among other mixing ratios, e.g., $r = 0.25$, 0.5, 4 and WPI as well. This similarly can be attributed to the cooperative adsorption of WPI and ALG at the air-water interface when intramolecular soluble complexes are formed, which leads to a thick and viscoelastic interfacial film at the air-water interface. The interfacial mechanical results are consistent with the maximum foam stability observed at $r = 1$ at pH 4.0 (Fig. 4b). It should be noted that the *E* values of the intramolecular soluble complexes at pH 4.0 and with $r = 1$ and 2 are relatively lower than those of the mixtures at pH 7.0 with higher *r*, although the formers exhibit higher foam stability. This might be due to the fact that the foam stability is not always fully determined by the interfacial mechanical property (Wouters, et al., 2017), but also the rheological properties such as the viscosity of the continuous phase of the bubbles. As shown in Fig. 6b and discussed above, intramolecular soluble polymers ($r = 1$ and 2) exhibited higher viscosity, which

probably reduce the water drainage between the bubbles and improve the stability of the foams. (Koehler, et al., 2000).

3.6. Interfacial microstructures

The microstructures of the interfacial films formed by WPI/ALG mixtures at the air-water interface were visualized using AFM. Fig. 8 compares the interfacial microstructures of WPI and WPI/ALG at pH = 7.0 and 4.0 and with r = 1 and 0.5. The WPI at pH 7.0 exists in the form of small globular aggregates at the air-water interface (Fig. 8a), while at pH 4.0 WPI shows a slight tendency of aggregation and forms a relatively more homogenous film (Fig. 8d). This might be due to the higher zeta potential of WPI at pH 7.0, yielding a stronger electrostatic repulsion between WPI molecules at the interface. At pH 7.0 and r = 1 and 0.5, where no electrostatic complexation occurs, WPI/ALG mixtures exhibit a dispersed interfacial morphology in which the linear structure of ALG and globular structure of WPI seem to coexist (Figs. 8b and 8c). The structures however change significantly at pH 4.0 where intramolecular soluble complexes are formed between WPI and ALG (Figs. 8e and 8f). Association between WPI and ALG can be clearly visualized. In contrast with pH 4.0 and r = 0.5, the mixture with r = 1 produces a thicker and more continuous network structure at the air-water interface. The interfacial structure formed by the former appears to be more dispersed. It indicates that the intramolecular soluble complex at its stoichiometry, i.e., r = 1, tends to produce a more homogenous and complete interfacial film at the air-water interface. This supports the results of viscosity shown in Fig. 6 and interfacial adsorption shown in Fig. 7 and the foam stability shown in Fig 4. The interfacial advantage of WPI/ALG intramolecular soluble complex at its stoichiometry is multifaceted, and includes: 1) high surface activity possibly due to the partial denaturation of WPI induced by electrostatic complexation; 2) high viscosity that retards the foam drainage rate; 3)

adsorption of WPI/ALG in a cooperative mechanism; 4) nearly electroneutrality that facilities the deposition and structural arrangement at the interface; 5) stable soluble complex that benefits the stabilization of the interface.

(Fig. 8. here)

4. Conclusions

The relationship between electrostatic interaction of WPI/ALG and the resulting foaming properties was investigated by constructing phase diagram, characterizing foam capacity and stability as well as visualizing interfacial microstructures. The results show that WPI/ALG complexes in different phase regions have similar foam capacity but significantly different foam stability. In the phase regions where no electrostatic complexation occurs, e.g., pH 7.0 and 0.5, the foam stability of WPI/ALG is mainly dominated by the protein component, and decreases with decreasing mixing ratio *r*. In the stable region of intramolecular soluble complexes, the electrostatic complexation between WPI and ALG yields the best foam stability, when the mixing ratio *r* is close to the stoichiometry, i.e., at *r* = 1 and 2. Under this particular condition, the half-life of the foams can be as long as 1 hour, nearly doubling that of pure WPI, even at a very low WPI/ALG concentration of 1mg/mL. Deviation from the particular phase region, however, leads to a degradation in foaming performance of WPI/ALG. The foaming properties are well supported by the results of viscosity and interfacial adsorption and microstructures, manifesting the interfacial advantage of the intramolecular soluble complexes. The study overall demonstrates an interesting approach to the stabilization of the air-water interface by protein/polysaccharide intramolecular electrostatic complex and their potential application in the food industry as superior foaming agent.

Acknowledgments

The research was supported by the grants from the National Natural Science Foundation of China (31671811, 31571797), the State Key Research and Development Plan "Modern food processing and food storage and transportation technology and equipment" (No. 2017YFD0400200), and the Science and Technology Commission of Shanghai Municipality (No.18JC1410801).

References

Akkermans, C., Goot, A. J. V. D., Venema, P., Linden, E. V. D., & Boom, R. M. (2008). Properties of protein fibrils in whey protein isolate solutions: microstructure, flow behaviour and gelation. *International Dairy Journal, 18*(10-11), 1034-1042.

Bals, A., & Kulozik, U. (2003). Effect of pre-heating on the foaming properties of whey protein isolate using a membrane foaming apparatus. *International Dairy Journal, 13*(11), 903-908.

Cao, Y., Li, S., Fang, Y., Nishinari, K., & Phillips, G. O. (2016). Conformational transition of polyelectrolyte as influenced by electrostatic complexation with protein. *Biomacromolecules, 17*(12), 3949-3956.

Castellani, O., Al-Assaf, S., Axelos, M., Phillips, G. O., & Anton, M. (2010). Hydrocolloids with emulsifying capacity. Part 2-adsorption properties at the N-hexadecane-water interface. *Food Hydrocolloids, 24*(2), 121-130.

Castellani, O., Gaillard, C., Vié, V., Al-Assaf, S., Axelos, M., Phillips, G. O., & Anton, M. (2010). Hydrocolloids with emulsifying capacity. Part 3 – adsorption and structural properties at the air–water surface. *Food Hydrocolloids, 24*(2), 131-141.

Castellani, O., Guibert, D., Al-Assaf, S., Axelos, M., Phillips, G. O., & Anton, M. (2010). Hydrocolloids with emulsifying capacity. Part 1 - emulsifying properties and interfacial characteristics of conventional (acacia senegal (L.) willd. var. senegal) and matured (acacia (sen) super gum™) acacia senegal. *Food Hydrocolloids, 24*(2), 193-199.

Davis, J. P., & Foegeding, E. A. (2004). Foaming and interfacial properties of polymerized whey protein isolate. *Journal of Food Science, 69*(5), 404-410.

Dickinson, E. (2010). Food emulsions and foams: stabilization by particles. *Current Opinion in Colloid & Interface Science, 15*(1), 40-49.

Dombrowski, J., Gschwendtner, M., & Kulozik, U. (2017). Evaluation of structural characteristics determining surface and foaming properties of β-lactoglobulin aggregates. *Colloids & Surfaces A Physicochemical & Engineering Aspects, 516*, 286-295.

Draget, K. I., Phillips, G. O., & Williams, P. A. (2009). Alginates. *Handbook of Hydrocolloids*, 379-396.

Foegeding, E. A., Luck, P. J., & Davis, J. P. (2006). Factors determining the physical properties of protein foams. *Food Hydrocolloids, 20*(2-3), 284-292.

Hill, C., & Eastoe, J. (2017). Foams: From nature to industry. *Adv Colloid Interface Sci, 247*, 496-513.

Jarpa-Parra, M., Tian, Z., Temelli, F., Zeng, H., & Chen, L. (2016). Understanding the stability mechanisms of lentil legumin-like protein and polysaccharide foams. *Food Hydrocolloids, 61*, 903-913.

Jordens, S., Isa, L., Usov, I., & Mezzenga, R. (2013). Non-equilibrium nature of two-dimensional isotropic and nematic coexistence in amyloid fibrils at liquid interfaces. *Nat Commun, 4*(5), 1917.

Koehler, S. A., Sascha Hilgenfeldt, & Stone, H. A. (2000). A generalized view of foam drainage: experiment and theory. *Langmuir, 16*(15), 6327-6341.

Kuropatwa, M., Tolkach, A., & Kulozik, U. (2009). Impact of pH on the interactions between whey and egg white proteins as assessed by the foamability of their mixtures. *Food Hydrocolloids, 23*(8), 2174-2181.

Langevin, D., Saintjalmes, A., Marze, S., Cox, S., Hutzler, S., Drenckhan, W., Weaire, D., Caps, H., Vandewalle, N., & Adler, M. (2005). Hydrodynamics of wet foams.

Li, X., Fang, Y., Al-Assaf, S., Phillips, G. O., & Jiang, F. (2012). Complexation of bovine serum albumin and sugar beet pectin: stabilising oil-in-water emulsions. *Journal of Colloid Interface Science, 388*(1), 103-111.

Li, X., Fang, Y., Al-Assaf, S., Phillips, G. O., Yao, X., Zhang, Y., Zhao, M., Zhang, K., & Jiang, F. (2012). Complexation of bovine serum albumin and sugar beet pectin: structural transitions and phase diagram. *Langmuir, 28*(27), 10164-10176.

Mekhloufi, G., Sanchez, C., & Renard, D. (2005). pH-induced structural transitions during complexation and coacervation of β-lactoglobulin and acacia gum. *Langmuir, 21*(1), 386-394.

Miquelim, J. N., Lannes, S. C. S., & Mezzenga, R. (2010). pH Influence on the stability of foams with protein–polysaccharide complexes at their interfaces. *Food Hydrocolloids, 24*, 398-405.

Murray, B. S. (2011). Rheological properties of protein films. *Current Opinion in Colloid & Interface Science, 16*(1), 27-35.

Narchi, I., Vial, C., & Djelveh, G. (2009). Effect of protein–polysaccharide mixtures on the continuous manufacturing of foamed food products. *Food Hydrocolloids, 23*(1), 188-201.

Oboroceanu, D., Wang, L., Magner, E., & Auty, M. A. E. (2014). Fibrillization of whey proteins

improves foaming capacity and foam stability at low protein concentrations. *Journal of Food Engineering, 121*(1), 102-111.

Oetjen, K., Bilke-Krause, C., Madani, M., & Willers, T. (2014). Temperature effect on foamability, foam stability, and foam structure of milk. *Colloids and Surfaces A: Physicochemical and Engineering Aspects, 460*, 280-285.

Peng, D., Yang, J., Li, J., Tang, C., & Li, B. (2017). Foams stabilized by β-lactoglobulin amyloid fibrils: effect of pH. *Journal of Agricultural and Food Chemistry, 65*(48), 10658-10665.

Piazza, L., Gigli, J., & Bulbarello, A. (2008). Interfacial rheology study of espresso coffee foam structure and properties. *Journal of Food Engineering, 84*(3), 420-429.

Ptaszek, P. (2013). The non-linear rheological properties of fresh wet foams based on egg white proteins and selected hydrocolloids. *Food Research International, 54*(1), 478-486.

Raikos, V., Campbell, L., & Euston, S. R. (2007). Effects of sucrose and sodium chloride on foaming properties of egg white proteins. *Food Research International, 40*(3), 347-355.

Rodríguez Patino, J. M., Carrera, S. C., & Rodríguez Niño, M. R. (2008). Implications of interfacial characteristics of food foaming agents in foam formulations. *Advances in Colloid & Interface Science, 140*(2), 95-113.

Rodríguez Patino, J. M., & Pilosof, A. M. R. (2011). Protein–polysaccharide interactions at fluid interfaces. *Food Hydrocolloids, 25*(8), 1925-1937.

Ruíz Henestrosa, V. P., Carrera-Sánchez, C., & Patino, J. M., Rodríguez. (2008). Effect of sucrose on functional properties of soy globulins: adsorption and foam characteristics. *Journal of Agricultural and Food Chemistry, 56*(7), 2512-2521.

Sadahira, M. S., Lopes, F. C., Rodrigues, M. I., Yamada, A. T., Cunha, R. L., & Netto, F. M. (2015). Effect of pH and interaction between egg white protein and hydroxypropymethylcellulose in

bulk aqueous medium on foaming properties. *Carbohydr Polym, 125*, 26-34.

Sadahira, M. S., Rodrigues, M. I., Akhtar, M., Murray, B. S., & Netto, F. M. (2016). Effect of egg white protein-pectin electrostatic interactions in a high sugar content system on foaming and foam rheological properties. *Food Hydrocolloids, 58*, 1-10.

Seyrek, E., Dubin, P. L., Tribet, C., & Gamble, E. A. (2003). Ionic strength dependence of protein-polyelectrolyte interactions. *Biomacromolecules, 4*(2), 273-282.

Stender, E. G. P., Khan, S., Ipsen, R., Madsen, F., Hägglund, P., Hachem, M. A., Almdal, K., Westh, P., & Svensson, B. (2018). Effect of alginate size, mannuronic/guluronic acid content and pH on particle Size, thermodynamics and composition of complexes with β-lactoglobulin. *Food Hydrocolloids, 75*, 157-163.

Su, C., Feng, Y., Jing, Y., Zhang, Y., Gao, Z., Meng, Z., Nan, Y., Nishinari, K., & Fang, Y. (2018). Effect of sodium alginate on the stability of natural soybean oil body emulsions. *RSC Advances, 8*(9), 4731-4741.

Vaclavik, V. A., & Christian, E. W. (2008). Food emulsions and foams. In *Essentials of food science* (pp. 311-327). New York, USA: Springer science business media.

van den Berg, M., Jara, F. L., & Pilosof, A. M. R. (2015). Performance of egg white and hydroxypropylmethylcellulose mixtures on gelation and foaming. *Food Hydrocolloids, 48*, 282-291.

van Kempen, S. E., Schols, H. A., Van, d. L. E., & Sagis, L. M. (2013). Non-linear surface dilatational rheology as a tool for understanding microstructures of air/water interfaces stabilized by oligofructose fatty acid esters. *Soft Matter, 9*(40), 9579-9592.

Vinayahan, T., ., Williams, P. A., & Phillips, G. O. (2010). Electrostatic interaction and complex formation between gum arabic and bovine serum albumin. *Biomacromolecules, 11*(12),

3367-3374.

Wan, Z., Yang, X., & LM, S. (2016). Nonlinear surface dilatational rheology and foaming behavior of p rotein and Protein Fibrillar Aggregates in the Presence of Natural Surfactant. *Langmuir, 32*(15), 3679-3690.

Wan, Z., Yang, X., & Sagis, L. M. C. (2016). Contribution of long fibrils and peptides to surface and foaming behavior of soy protein fibril system. *Langmuir, 32*(32), 8092-8101.

Weinbreck, F., De, V. R., Schrooyen, P., & de Kruif, C. G. (2003). Complex coacervation of whey proteins and gum arabic. *Biomacromolecules, 4*(2), 293-303.

Weinbreck, F., Nieuwenhuijse, H., Robijn, G. W., & de Kruif, C. G. (2004). Complexation of whey proteins with carrageenan. *Journal of Agricultural & Food Chemistry, 52*(11), 3550-3555.

Wouters, A. G. B., Fierens, E., Rombouts, I., Brijs, K., Joye, I. J., & Delcour, J. A. (2017). Exploring the relationship between structural and air-water interfacial properties of wheat (triticum aestivum L.) gluten hydrolysates in a food system relevant pH range. *Journal of Agricultural & Food Chemistry, 65*(6), 1263-1271.

Yao, X., Xiang, S., Nie, K., Gao, Z., Zhang, W., Fang, Y., Nishinari, K., Phillips, G. O., & Jiang, F. (2016). Whey protein isolate/gum arabic intramolecular soluble complexes improving the physical and oxidative stabilities of conjugated linoleic acid emulsions. *RSC Advances, 6*(18), 14635-14642.

Ye, A., & Flanagan, J., H. (2006). Formation of stable nanoparticles via electrostatic complexation between sodium caseinate and gum arabic. *Biopolymers, 82*(2), 121-133.

Zang, D., Li, L., Di, W., Zhang, Z., Ding, C., Chen, Z., Shen, W., Binks, B. P., & Geng, X. (2018). Inducing drop to bubble transformation via resonance in ultrasound. *Nat Commun, 9*(1), 3546.

Figure Captions

Fig. 1. (a) ζ-potential as a function of pH for WPI/ALG with varying mixing ratios (*r*). (b) Isoelectric point (IEP) plotted against *r*. The logarithmic x-axis in (b) was broken for including the data points of pure WPI and ALG (indicated in yellow). The total biopolymer concentration was fixed at 0.1% w/w.

Fig. 2. (a) Evolution of the scattered light intensity at 173° (I_{173}, Δ) and turbidity at 500 nm (τ, □) during GDL-induced acidification and turbidity measured at 500 nm (○) during HCl titration for WPI/ALG mixture with r = 1. (b) Phase diagram of WPI/ALG mixtures in a pH−composition coordinate: Δ (pH_c), □ (pH_φ), and ○ (pH_d). The dashed line indicates the IEP of pure WPI.

Fig. 3. Foam capacity of WPI/ALG mixtures at pHs 7.0, 4.0 and 0.5 and with varying mixing ratio. The total biopolymer concentration was fixed at 0.1% w/w.

Fig. 4. (a) Foam formation and decay for WPI/ALG mixtures at pH 4.0 and various mixing ratios; (b) Comparison of foam half-life for WPI/ALG mixtures at different pHs and mixing ratios. The total biopolymer concentration was fixed at 0.1% w/w.

Fig. 5. Time evolution of air bubbles within foams formed by WPI/ALG mixtures at different pHs and mixing ratios: pH 7.0 (a); pH 4.0 (b) and pH 0.5 (c). The total biopolymer concentration was fixed at 0.1% w/w. Scale bars = 1 mm.

Fig. 6. Viscosity of WPI/ALG mixtures as a function of shear rate at different pHs and mixing ratios: pH 7.0 (a); pH 4.0 (b) and pH 0.5 (c). The total biopolymer concentration was fixed at 0.1% w/w.

Fig. 7. Time evolution of the surface tension at pHs 7.0 (a) and 4.0 (b) and the surface dilatational modulus at pHs 7.0 (c) and 4.0 (d) upon the adsorption of WPI/ALG on to the air-water interface at varying mixing ratios.

Fig. 8. AFM visualization of the interfacial films formed by WPI and WPI/ALG at the air-water interface at pH 7.0 and pH 4.0 and with different mixing ratios *r*. The total concentration of WPI and ALG was 0.01 mg/mL. The scale bars represent 400 nm.

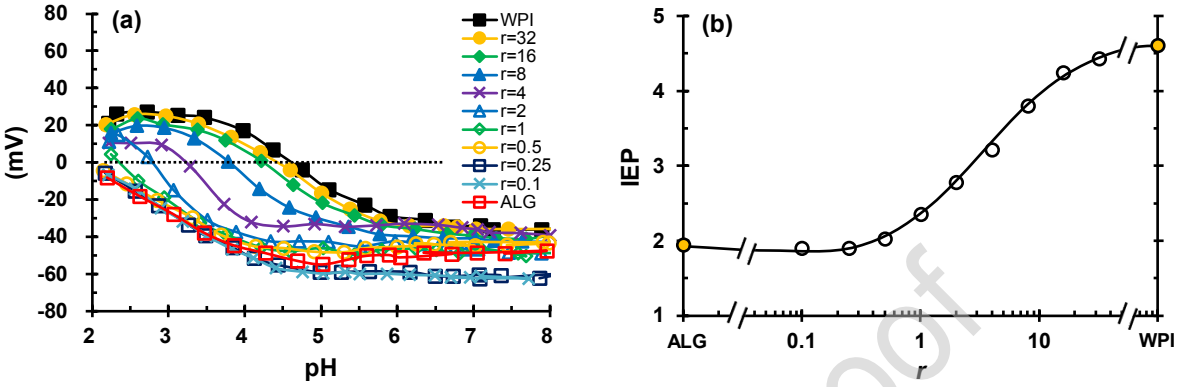

Fig. 1. (a) ζ-potential as a function of pH for WPI/ALG with varying mixing ratios (*r*). (b) Isoelectric point (IEP) plotted against *r*. The logarithmic x-axis in (b) was broken for including the data points of pure WPI and ALG (indicated in yellow). The total biopolymer concentration was fixed at 0.1% w/w.

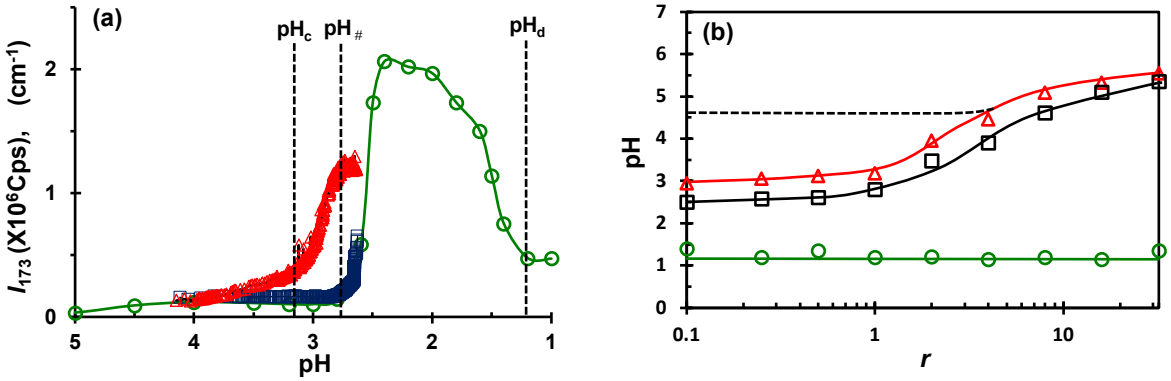

Fig. 2. (a) Evolution of the scattered light intensity at 173° (I_{173}, △) and turbidity at 500 nm (τ, □) during GDL-induced acidification and turbidity measured at 500 nm (○) during HCl titration for WPI/ALG mixture with r = 1. (b) Phase diagram of WPI/ALG mixtures in a pH−composition coordinate: △ (pH_c), □ (pH_φ), and ○ (pH_d). The dashed line indicates the IEP of pure WPI.

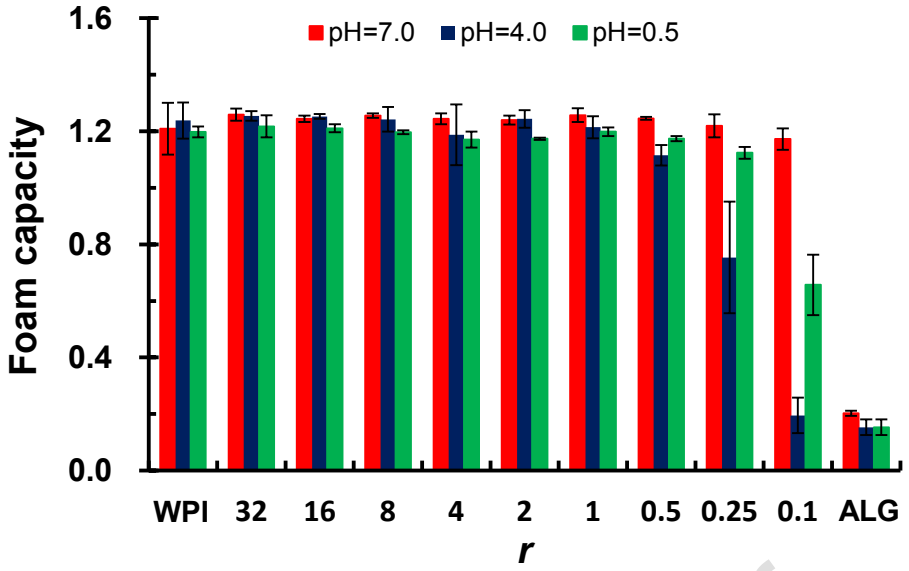

Fig. 3. Foam capacity of WPI/ALG mixtures at pHs 7.0, 4.0 and 0.5 and with varying mixing ratio. The total biopolymer concentration was fixed at 0.1% w/w.

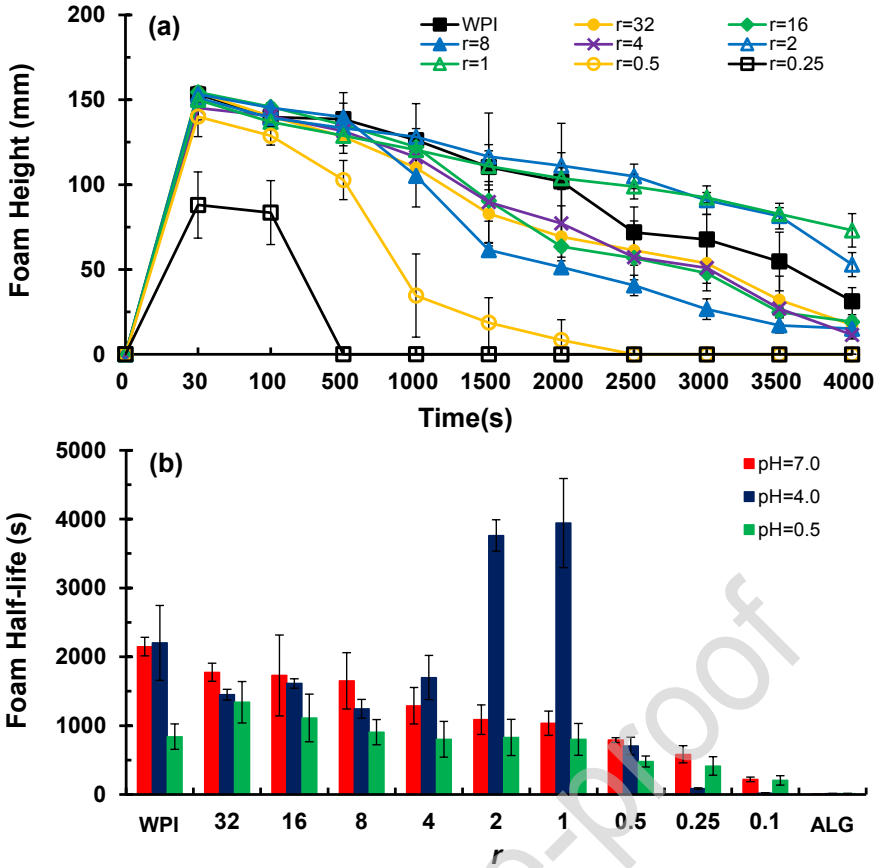

Fig. 4. (a) Foam formation and decay for WPI/ALG mixtures at pH 4.0 and various mixing ratios; (b) Comparison of foam half-life for WPI/ALG mixtures at different pHs and mixing ratios. The total biopolymer concentration was fixed at 0.1% w/w.

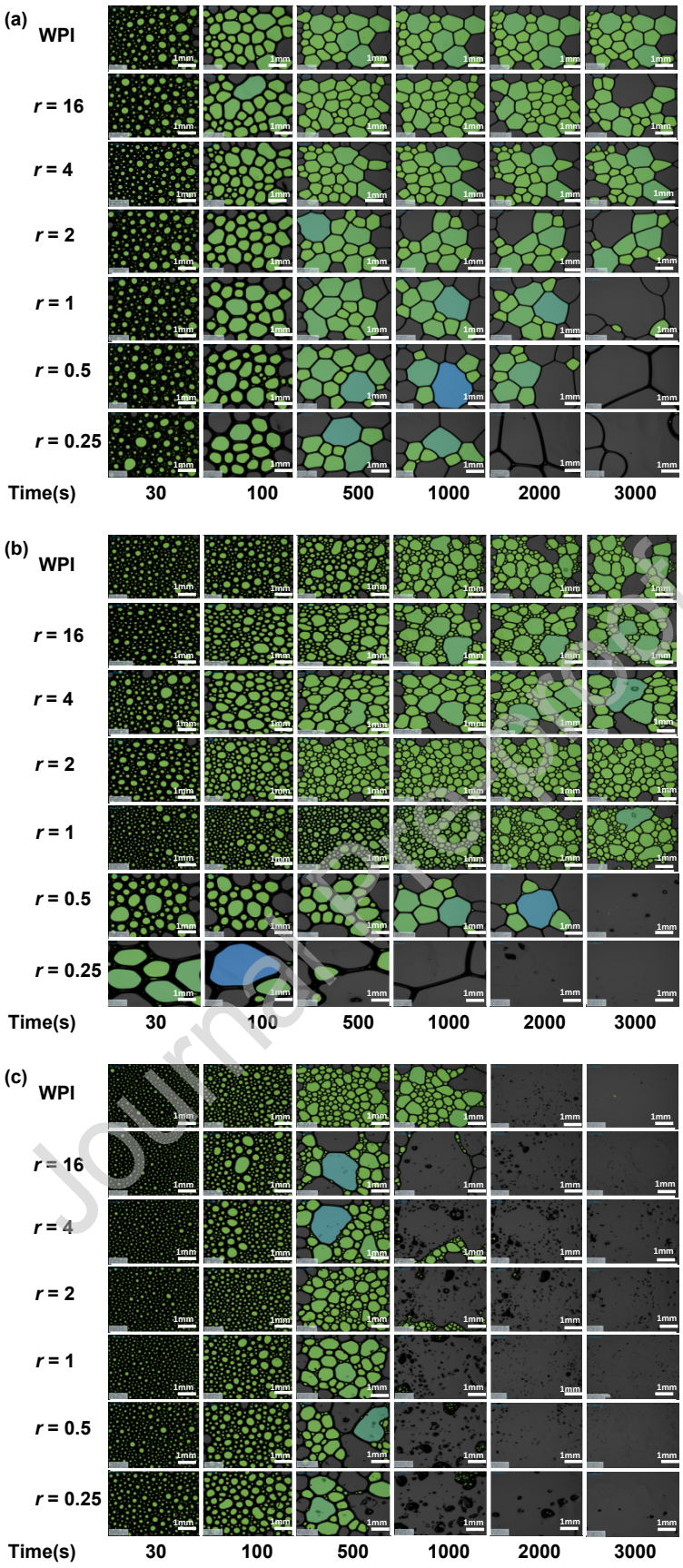

Fig. 5. Time evolution of air bubbles within foams formed by WPI/ALG mixtures at different pHs and mixing ratios: pH 7.0 (a); pH 4.0 (b) and pH 0.5 (c). The total biopolymer concentration was

fixed at 0.1% w/w. Scale bars = 1 mm.

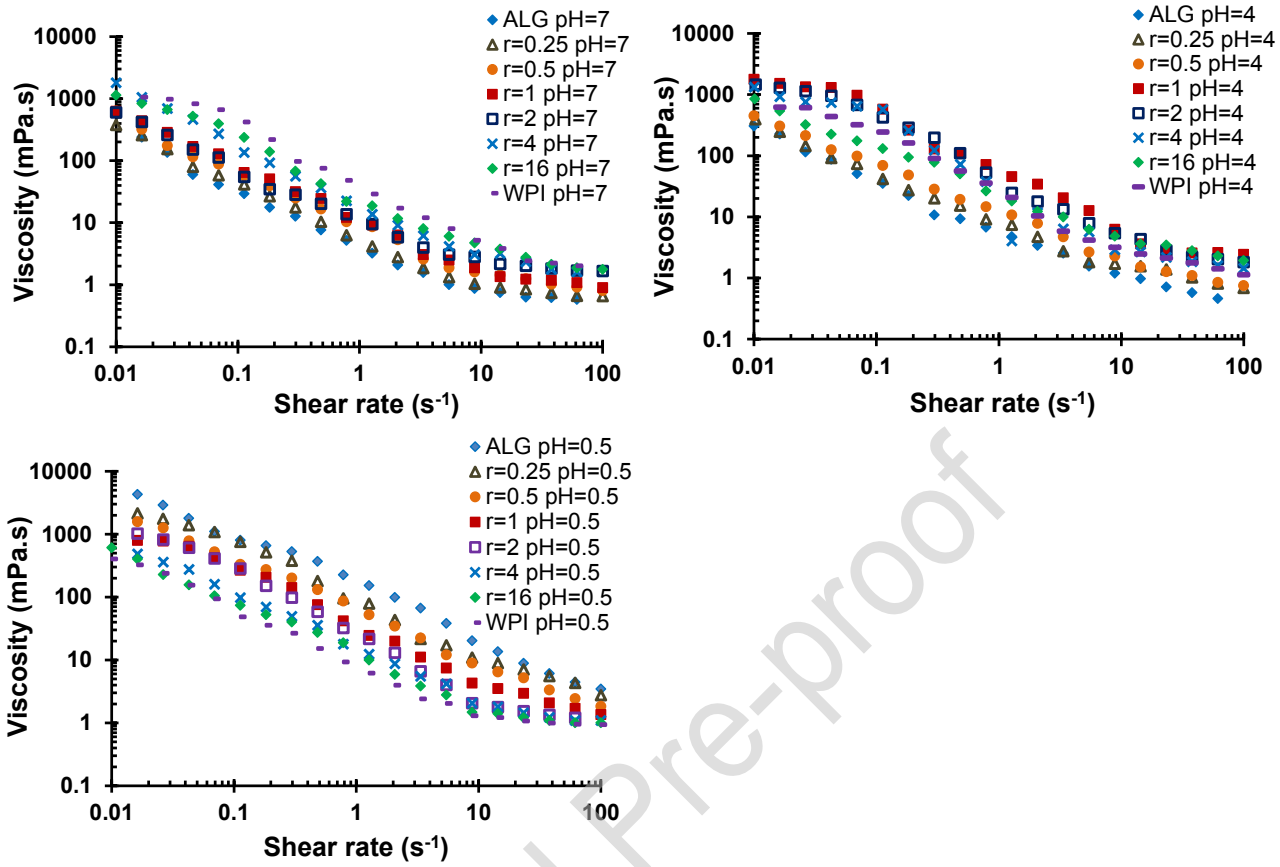

Fig. 6. Viscosity of WPI/ALG mixtures as a function of shear rate at different pHs and mixing ratios: pH 7.0 (a); pH 4.0 (b) and pH 0.5 (c). The total biopolymer concentration was fixed at 0.1% w/w.

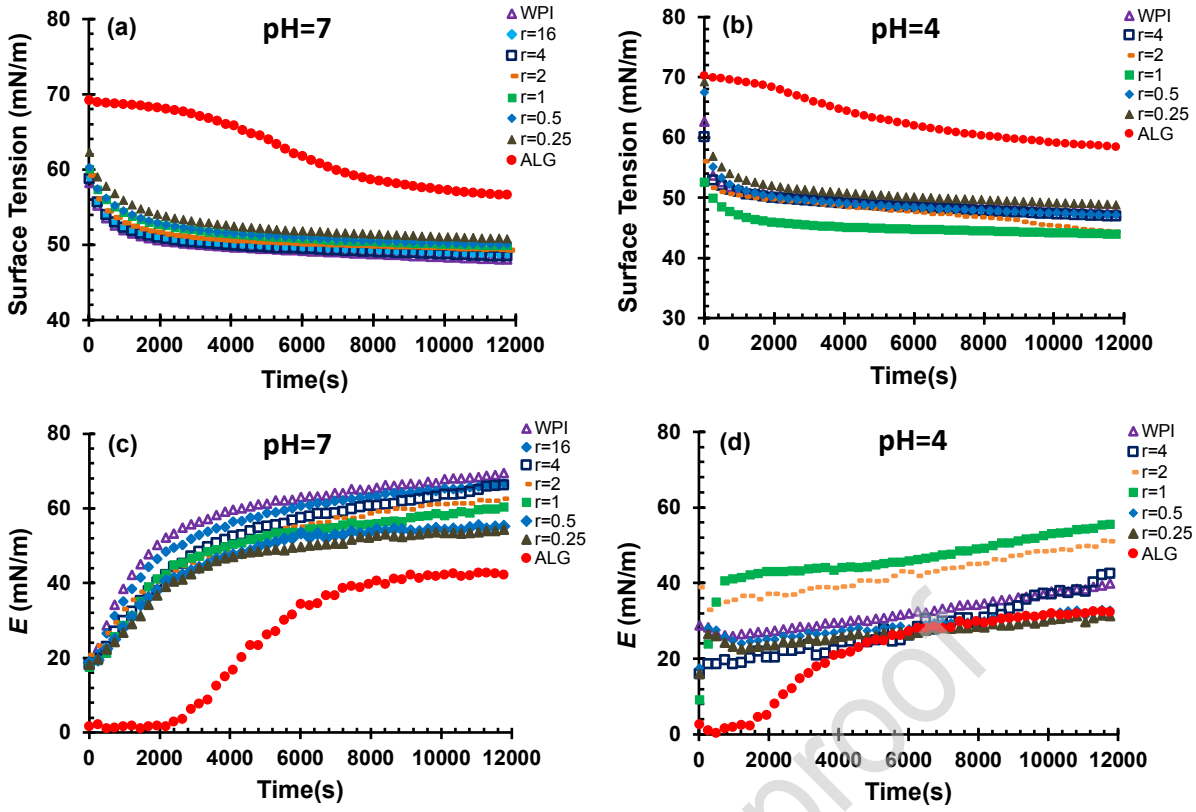

Fig. 7. Time evolution of the surface tension at pHs 7.0 (a) and 4.0 (b) and the surface dilatational modulus at pHs 7.0 (c) and 4.0 (d) upon the adsorption of WPI/ALG on to the air-water interface at varying mixing ratios.

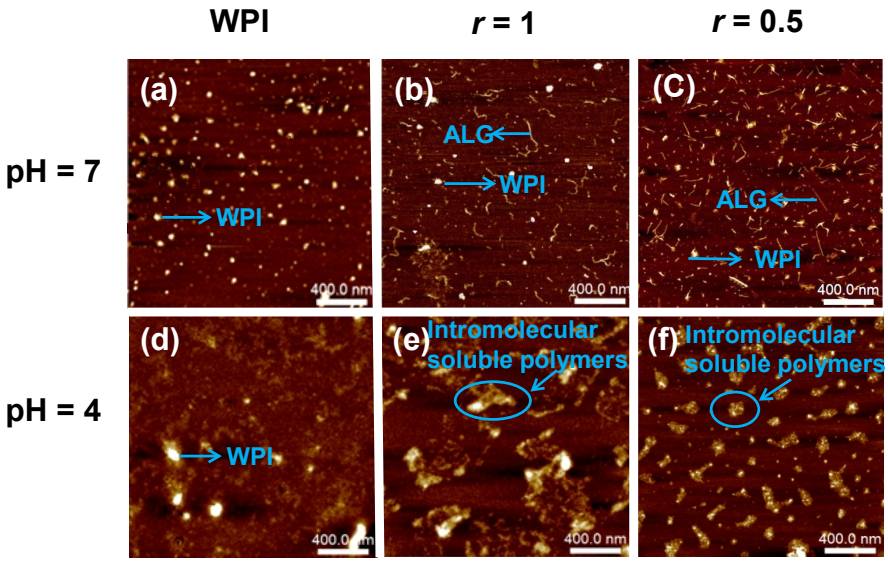

Fig. 8. AFM visualization of the interfacial films formed by WPI and WPI/ALG at the air-water interface at pH 7.0 and pH 4.0 and with different mixing ratios *r*. The corresponding components observed in each sample has been marked in the images. The total concentration of WPI and ALG was 0.01 mg/mL. The scale bars represent 400 nm.

The authors declare no conflict of interest.

Highlights

- The foaming properties of protein/polysaccharide mixtures were investigated.
- The foaming properties were closely related to the state of electrostatic complexes.
- Intramolecular soluble complexes at stoichiometry provided the best foam stability.
- The foaming properties were consistent with interfacial adsorption and structures.